Inorganic Chemistry Communications 50 (2014) 19–23

Contents lists available at ScienceDirect

Inorganic Chemistry Communications

journal homepage: www.elsevier.com/locate/inoche

# A 3-D framework based on mono-copper$^{II}$ substituted silicotungstate units $[Cu(dap)_2(H_2O)]_2[Cu(dap)_2][\alpha\text{-}SiW_{11}CuO_{39}]\cdot 2H_2O$

Jie Luo [a], Hailou Li [a], Xinxin Chen [b], Jianru Ma [c], Lijuan Chen [a], Junwei Zhao [a,*]

[a] Henan Key Lab of Polyoxometalate Chemistry, Institute of Molecule and Crystal Engineering, College of Chemistry and Chemical Engineering, Henan University, Kaifeng, Henan 475004, PR China
[b] Huaihe Hospital, Henan University, Kaifeng, Henan 475004, PR China
[c] Anyang Environmental Protection Testing Center, Anyang, Henan 455000, PR China

ARTICLE INFO

*Article history:*
Received 3 September 2014
Received in revised form 6 October 2014
Accepted 9 October 2014
Available online 13 October 2014

*Keywords:*
Polyoxometalate
Silicotungstate
3-D framework
Electrocatalysis

ABSTRACT

A 3-D mono-copper$^{II}$ substituted silicotungstate $[Cu(dap)_2(H_2O)]_2[Cu(dap)_2][\alpha\text{-}SiW_{11}CuO_{39}]\cdot 2H_2O$ (**1**) has been hydrothermally synthesized by reaction of $Na_{10}[A\text{-}\alpha\text{-}SiW_9O_{34}]\cdot 18H_2O$, $CuCl_2\cdot 2H_2O$, $LaCl_3$ and dap (dap = 1,2-diaminopropane) and characterized by elemental analyses, IR spectrum, thermogravimetric (TG) analysis, powder X-ray diffraction (PXRD) and single-crystal X-ray diffraction. To our knowledge, **1** represents the first 3-D four-connected framework with the Schläfli symbol of $6^4 \cdot 8 \cdot 10$ that is built by mono-copper$^{II}$ substituted silicotungstate units in polyoxometalate chemistry. The TG curve of **1** indicates two steps of weight loss between 25 and 750 °C. Furthermore, the solid-state electrochemical and electro-catalytic properties of **1** have been measured in 0.5 mol·L$^{-1}$ $Na_2SO_4 + H_2SO_4$ aqueous solution by entrapping it in a carbon paste electrode. **1** displays evident electro-catalytic activities toward the nitrite and bromated reduction.

© 2014 Elsevier B.V. All rights reserved.

The continuous interest in search and synthesis of novel transition-metal (TM) or lanthanide (Ln) substituted polyoxometalates (POMs) with unique structures and properties are dominantly driven by their fascinating structural and compositional diversities and manifold potential applications in catalysis, medicine, biology and material science [1–4]. Currently, the integration of lacunary POM segments with various TM or Ln cations has led to a large number of TM or Ln cations substituted POMs. Within this field, silicotungstate (ST) as one important subfamily of POMs have made great progress and some interesting TM or Ln substituted STs are as follows: $[Mn_{19}(OH)_{12}(SiW_{10}O_{37})_6]^{34-}$ [5], $[\{K(H_2O)\}_2\{(\mu_3\text{-}H_2O)M(H_2O)\}(\gamma\text{-}Si_2W_{20}O_{70})]^{8-}$ (M = $Mn^{2+}$, $Co^{2+}$, $Ni^{2+}$) [6], $[Zr_6/Hf_6(O_2)_6(OH)_6(\gamma\text{-}SiW_{10}O_{36})_3]^{18-}$ [7], $[Mn^{III}_2Mn^{II}_4(\mu_3\text{-}O)_2(H_2O)_4(B\text{-}\beta\text{-}SiW_8O_{31})(B\text{-}\beta\text{-}SiW_9O_{34})(\gamma\text{-}SiW_{10}O_{36})]^{18-}$ [8], $[Ni_6(\mu_3\text{-}OH)_3(H_2O)_9SiW_9O_{34}]_2^{2-}$ [9], $[Ln_2(H_2O)_7Si_2W_{18}O_{66}]^{10-}$ (Ln = $Gd^{3+}$, $Tb^{3+}$, $Ho^{3+}$) [10], $TBA_6H_4[\{RE(H_2O)_2(acetone)\}_2\{\gamma\text{-}SiW_{10}O_{36}\}_2]\cdot n(acetone)\cdot 2H_2O$ (RE = $Y^{3+}$, $Nd^{3+}$, $Eu^{3+}$, $Gd^{3+}$, $Tb^{3+}$, $Dy^{3+}$) [11] and $\{Na(H_2O)_3[Lu(pydc)(H_2O)_3]_3\}[SiW_{12}O_{40}]\cdot 26.5H_2O$ [12]. The Keggin-type trilacunary $[A\text{-}\alpha\text{-}SiW_9O_{34}]^{10-}$ as an important ST precursor, which was first discovered by Hervé and Tézé in 1977 [13], has attracted increasing attention, because it has six unsaturated oxygen atoms available for coordination with positive metal cations. It should be pointed out that $[A\text{-}\alpha\text{-}SiW_9O_{34}]^{10-}$ is easily prepared in a one-step process in high yield and can isomerize to $[B\text{-}\alpha\text{-}SiW_9O_{34}]^{10-}$, $[\alpha\text{-}SiW_{11}O_{39}]^{8-}$, $[\alpha\text{-}SiW_{12}O_{40}]^{4-}$ and $[\beta\text{-}SiW_8O_{31}]^{10-}$ intermediate phases during the course of the reaction. Recently, we have launched investigations on the reactions of this precursor with copper and Ln cations in the presence of organic components under hydrothermal conditions. Firstly, we successfully synthesized a class of unique 1-D double-chain ST-based Cu–Ln heterometallic hybrids $[Cu(dap)_2(H_2O)]_2\{Cu(dap)_2[\alpha\text{-}H_2SiW_{11}O_{39}Ln(H_2O)_3]_2\}\cdot xH_2O$ [Ln = $Ce^{3+}$, x = 9; Ln = $Pr^{3+}$, x = 10; Ln = $Nd^{3+}$, x = 10; Ln = $Sm^{3+}$, x = 10; Ln = $Eu^{3+}$, x = 10; Ln = $Gd^{3+}$, x = 9; Ln = $Tb^{3+}$, x = 8; Ln = $Dy^{3+}$, x = 8; Ln = $Er^{3+}$, x = 9] [14] and $[Cu(dap)_2(H_2O)]_2\{Cu(dap)_2[\alpha\text{-}H_2SiW_{11}O_{39}Y(H_2O)_2]_2\}\cdot 10H_2O$ [15]. Subsequently, three 3-D organic–inorganic hybrid heterometallic polyoxotungstates assembled from 1:2-type $[Ln(\alpha\text{-}SiW_{11}O_{39})_2]^{13-}$ silicotungstates and $[Cu(dap)_2]^{2+}$ linkers NaH $[Cu(dap)_2(H_2O)][Cu(dap)_2]_{4.5}[Ln(\alpha\text{-}SiW_{11}O_{39})_2]\cdot 7H_2O$ (Ln = $Sm^{3+}$, $Dy^{3+}$, $Gd^{3+}$) were isolated [16]. As a part of our continuous work, unexpectedly a novel 3-D framework based on mono-Cu$^{II}$ substituted ST units $[Cu(dap)_2(H_2O)]_2[Cu(dap)_2][\alpha\text{-}SiW_{11}CuO_{39}]\cdot 2H_2O$ (**1**) has been synthesized by reaction of $Na_{10}[A\text{-}\alpha\text{-}SiW_9O_{34}]\cdot 18H_2O$, $CuCl_2\cdot 2H_2O$, $LaCl_3$ and dap under hydrothermal conditions and characterized by elemental analyses, IR spectrum and single-crystal X-ray diffraction. Its TG behavior has been investigated. Moreover, the results of electro-catalytic experiments indicate that **1** displays apparent electro-catalytic activities toward the reduction of nitrite and bromate.

**1** was prepared hydrothermally by a mixture of $Na_{10}[A\text{-}\alpha\text{-}SiW_9O_{34}]\cdot 18H_2O$ (0.298 g, 0.106 mmol), $CuCl_2\cdot 2H_2O$ (0.078 g, 0.457 mmol), $LaCl_3$ (0.068 g, 0.277 mmol), dap (0.10 mL, 0.901 mmol) and $H_2O$ (5 mL, 278 mmol). The mixture was stirred for 2 h, sealed in a 25 mL Teflon-lined steel autoclave, kept at 160 °C for 6 days and then slowly cooled to room temperature. Purple needle-like crystals were collected by filtration, washed with distilled water

* Corresponding author.
*E-mail address:* zhaojunwei@henu.edu.cn (J. Zhao).

http://dx.doi.org/10.1016/j.inoche.2014.10.003
1387-7003/© 2014 Elsevier B.V. All rights reserved.

and dried in air at ambient temperature. Yield: ca. 33% (based on $Na_{10}[A\text{-}\alpha\text{-}SiW_9O_{34}]\cdot 18H_2O$). Anal. calcd. (found %) for $C_{18}H_{68}Cu_4N_{12}O_{43}SiW_{11}$ (**1**): C 6.28 (6.43), H 1.99 (1.86), N 4.88 (4.64), Cu 7.38 (7.22), Si 0.82 (0.94), and W 58.70 (58.92). Though $Na_{10}[A\text{-}\alpha\text{-}SiW_9O_{34}]\cdot 18H_2O$ was employed during the course of preparing **1**, the $[\alpha\text{-}SiW_{11}O_{39}]^{8-}$ segment exists in **1**. However, when $Na_{10}[A\text{-}\alpha\text{-}SiW_9O_{34}]\cdot 18H_2O$ was replaced by $K_8[\alpha\text{-}SiW_{11}O_{39}]\cdot 13H_2O$ under the similar conditions, **1** can't be obtained, which is indicative of the necessity of the conversion of $[A\text{-}\alpha\text{-}SiW_9O_{34}]^{10-} \rightarrow [\alpha\text{-}SiW_{11}O_{39}]^{8-}$ in the formation of **1**. This conversion has been previously encountered in the preparations of ST-based Cu–Ln heterometallic derivatives [14–16]. Additionally, albeit $LaCl_3$ was used as a starting reactant in the reaction, there was no $La^{III}$ ion in **1**. The paralleling experiments were conducted in the absence of $LaCl_3$, but **1** was not formed, which indicates that $LaCl_3$ plays a certain synergistic action with other constituents in the formation of **1** though its specific role was not well understood in the reaction. Actually, in the preparation of novel organic–inorganic hybrid sandwich-type germanotungstate $[enH_2]_8[Fe_4(en)(\alpha\text{-}GeW_9O_{34})_2][Fe_4(en)_2(\alpha\text{-}GeW_9O_{34})_2]\cdot en\cdot 14H_2O$ by reaction of $K_8Na_2[A\text{-}\alpha\text{-}GeW_9O_{34}]\cdot 25H_2O$, $FeCl_3$ and $Ce(NH_4)_4(SO_4)_4\cdot 4H_2O$ in the participation of ethylenediamine (en), although $Ce(NH_4)_4(SO_4)_4\cdot 4H_2O$ was used as a reactant, no $Ce^{4+}$ ion was observed in this complex [17]. The paralleling experiments showed that the amorphous powder was afforded when $Ce(NH_4)_4(SO_4)_4\cdot 4H_2O$ was removed away from the reaction. Similar phenomena have been previously encountered during the course of preparing the hexa-$Cu^{II}$ substituted sandwich-type arsenotungstates $[Cu(en)_2(H_2O)]_2[Cu(en)_2][Cu_6(en)_2(H_2O)_2(B\text{-}\alpha\text{-}AsW_9O_{34})_2]\cdot en\cdot 9H_2O$ and $[Cu(dap)_2]_3[Cu_6(dap)_2(H_2O)_2(B\text{-}\alpha\text{-}AsW_9O_{34})_2]\cdot 4H_2O$ [18].

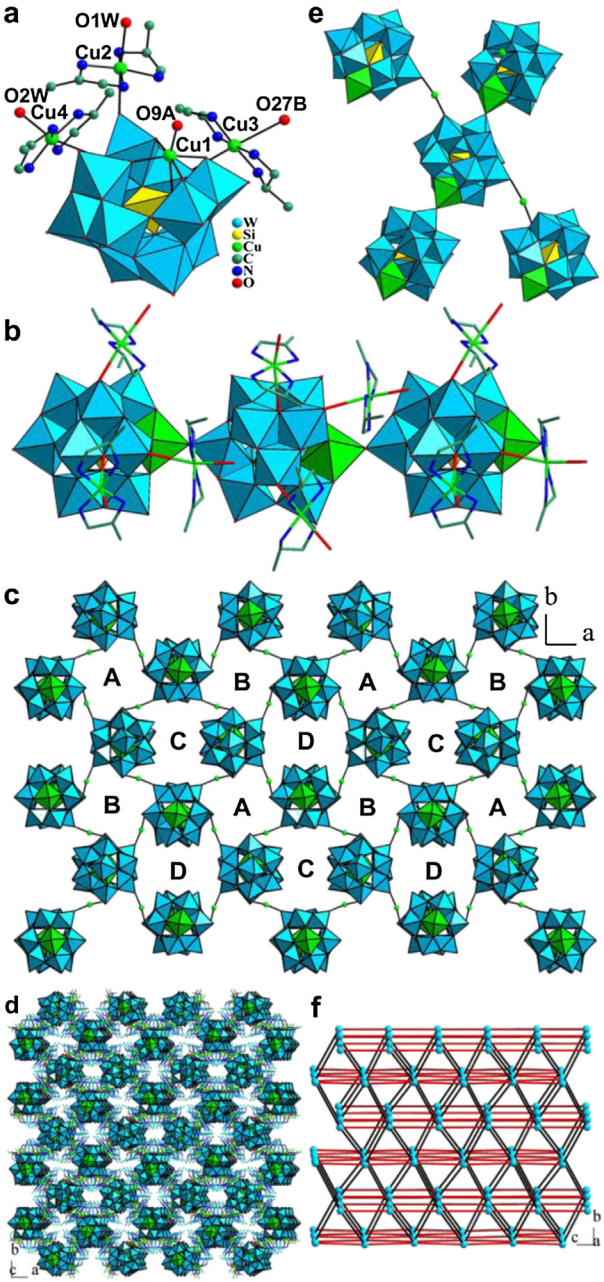


**Fig. 1.** (a) Ball-and-stick/polyhedral representation of the structural unit of **1** with the selected labeling scheme. Lattice water molecules and hydrogen atoms attached to carbon and nitrogen atoms are omitted for clarity. (b) The 1-D polymeric linear chain formed by $\{Cu(dap)_2(H_2O)]_2[Cu(dap)_2][\alpha\text{-}SiW_{11}CuO_{39}]\}$ structural units by virtue of Cu–O–W linkers. (c) The simplified 3-D framework viewed along the *c* axis. The $Cu2^{2+}$, $Cu4^{2+}$, dap and $H_2O$ are omitted for clarity. (d) The 3-D framework viewed along the *c* axis. (e) The connection motif between one $[\alpha\text{-}SiW_{11}CuO_{39}]^{6-}$ subunit and four adjacent identical $[\alpha\text{-}SiW_{11}CuO_{39}]^{6-}$ subunits. (f) The 4-connected 3-D topological framework.

The phase purity of **1** was characterized by the PXRD pattern of the bulk product (Fig. S1). The peak positions are in good agreement with each other, indicating the phase purity of the product. Single-crystal X-ray diffraction [19] indicates that **1** crystallizes in the tetragonal space group $I4_1cd$ and its molecular structural unit (Fig. 1a) is composed of one mono-$Cu^{II}$ substituted Keggin ST $[\alpha\text{-}SiW_{11}CuO_{39}]^{6-}$ moiety, one bridging $[Cu(dap)_2]^{2+}$ cation, two pendant $[Cu(dap)_2(H_2O)]^{2+}$ cations and two lattice water molecules. In **1**, there are four crystallographically independent $Cu^{2+}$ cations (Cu1, Cu2, Cu3 and Cu4). The oxidation states of copper cations can be confirmed by bond valence sum (BVS) calculations [20,21]. The BVS values of Cu1, Cu2, Cu3 and Cu4 cations are 2.30, 2.30, 1.98 and 2.27, respectively, which indicate that the oxidation states of all the copper cations are +2, which are further supported by the XPS spectrum (Fig. S2). The $Cu2p_{3/2}$ and $Cu2p_{1/2}$ binding energies of 933.3 and 952.8 eV are coincident with the previous results [22,23], confirming the presence of the $Cu^{2+}$ cations in **1**. The $Cu1^{2+}$ cation is embedded in the monovacant site of the $[\alpha\text{-}SiW_{11}O_{39}]^{8-}$ fragment creating the $[\alpha\text{-}SiW_{11}CuO_{39}]^{6-}$ moiety with one $\{CuW_2O_{13}\}$ and three $\{W_3O_{13}\}$ trimers and exhibits a distorted $\{CuO_6\}$ octahedral geometry with Cu–O distances of 1.95(3)–2.26(2) Å. The pendant $[Cu2(dap)_2(H_2O)]^{2+}$ and $[Cu4(dap)_2(H_2O)]^{2+}$ cations graft to the $[\alpha\text{-}SiW_{11}CuO_{39}]^{6-}$ moiety through a terminal or bridging oxygen atom and both adopt the elongated $\{CuO_2N_4\}$ octahedral geometry, where four nitrogen atoms from two bidentate dap ligands occupy the equatorial plane [Cu–N: 1.955(5)–2.006(5) Å] and a terminal or bridging oxygen atom from a $\{W_3O_{13}\}$ trimer and a water oxygen atom stand on two polar positions [Cu–O: 2.21(3)–3.106(22) Å]. The bridging $[Cu3(dap)_2]^{2+}$ cation also inhabits in an elongated $\{CuO_2N_4\}$ octahedron, in which four nitrogen atoms from two bidentate dap ligands define the basal plane [Cu–N: 1.96(4)–2.13(3) Å] and two terminal oxygen atoms from two adjacent $[\alpha\text{-}SiW_{11}CuO_{39}]^{6-}$ moieties are situated on two axial sites [Cu–O: 2.523(23)–2.813(28) Å]. Notably, adjacent $\{Cu(dap)_2(H_2O)]_2[Cu(dap)_2][\alpha\text{-}SiW_{11}CuO_{39}]\}$ structural units are interconnected together through sharing terminal oxygen atoms by virtue of Cu–O–W linkers giving rise to the 1-D polymeric linear chain (Fig. 1b). This 1-D polymeric polyoxoanion linear chain is similar to that observed in $\{[Cu(en)_2(H_2O)]_2[Cu(en)_2][\alpha\text{-}SiCuW_{11}O_{39}]\}\cdot 5H_2O$ [24], which can be viewed as the result of the substitution of a water molecule on a $[\alpha\text{-}SiCuW_{11}(H_2O)O_{39}]^{6-}$ anion by a terminal oxygen atom on a $WO_6$ octahedron from the adjacent Keggin unit. More interestingly, neighboring 1-D polymeric polyoxoanion chains are joined together via the $[Cu3(dap)_2]^{2+}$ connectors constructing a 3-D extended framework (Figs. 1c, d, S3), in which each $[\alpha\text{-}SiCuW_{11}O_{39}]^{6-}$ moiety is combined with four identical $[\alpha\text{-}SiCuW_{11}O_{39}]^{6-}$ moieties by two Cu1–O–W linkers and two W–O–Cu3–O–W linkers (Fig. 1e). From Fig. 1c we can see that the stacking of $[\alpha\text{-}SiCuW_{11}O_{39}]^{6-}$ moieties along the *c* axis can generate square-

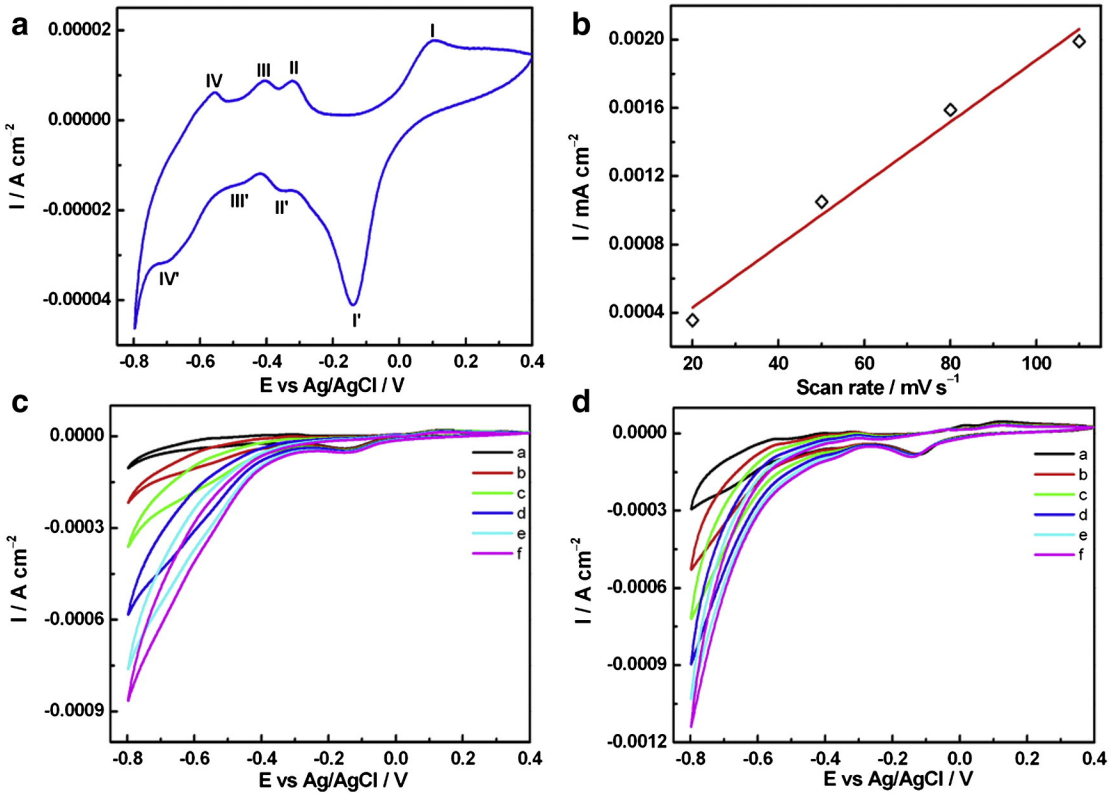


**Fig. 2.** (a) Cyclic voltammogram of **1**-CPE in pH = 0.46, 0.5 mol·L$^{-1}$ $Na_2SO_4 + H_2SO_4$ aqueous solution. (b) Variation of cathodic (II) peak currents of the $W^{VI}$-based wave with the scan rate for **1**-CPE. (c) Cyclic voltammograms of **1**-CPE in pH = 0.46, 0.5 mol L$^{-1}$ $Na_2SO_4 + H_2SO_4$ aqueous solution containing various concentrations (a: $1 \times 10^{-3}$, b: $3 \times 10^{-3}$, c: $5 \times 10^{-2}$, d: $7 \times 10^{-3}$, e: $9 \times 10^{-3}$, f: $11 \times 10^{-3}$) of $NaNO_2$. (d) Cyclic voltammograms of **1**-CPE in pH = 0.46, 0.5 mol L$^{-1}$ $Na_2SO_4 + H_2SO_4$ aqueous solution containing various concentrations (a: $1 \times 10^{-3}$, b: $3 \times 10^{-3}$, c: $5 \times 10^{-2}$, d: $7 \times 10^{-3}$, e: $9 \times 10^{-3}$, f: $11 \times 10^{-3}$) of $NaBrO_3$.

shaped (A and B) and elliptical (C and D) channels. The square-shaped A and B channels can be looked on as the mirror symmetry regardless of the spatial orientation of the $\{Cu1O_6\}$ octahedra on $[\alpha\text{-}SiCuW_{11}O_{39}]^{6-}$ moieties and their sizes are ca. 13 × 13 Å whereas the elliptical C channels are rotated by 90° to transfer the D channels and their sizes are ca. 15 × 12 Å. Obviously, theses square-shaped and elliptical channels are mainly filled by hydrophobic dap ligands from $[Cu(dap)_2(H_2O)]^{2+}$ and $[Cu(dap)_2]^{2+}$ cations (Fig. 1d), which may be the reason why the number of lattice water molecules in **1** is small. So far as we know, **1** stands for the rare 3-D framework built by mono-copper$^{II}$ substituted ST units in POM chemistry although a 2-D mono-Sm$^{III}$ substituted ST $H\{[Sm(H_2O)_{5.5}(DMF)_{0.5}]_2[Sm(H_2O)_2(DMF)][Sm(H_2O)_3(\alpha\text{-}SiW_{11}O_{39})]_2\}$ was reported by Niu et al. in 2006 [25]. From the viewpoint of topology, the 3-D networks can be simplified to the node-and-spacer representation, which facilitates to understand those complicated structures by crystal engineering. The circuit symbols and Schläfli (vertex) notations can be used to describe topologies and facilitate comparison of networks of different compositions and metrics. The 3-D extended framework of **1** is a 4-connected 3-D network, where each structural unit functions as a 4-connected node. A topological analysis of this framework was performed with OLEX [26]. The long topological (O'Keeffe) vertex symbol is $6 \cdot 8_2 \cdot 6 \cdot 6 \cdot 10_2 \cdot 6$ and the short vertex (Schläfli) symbol is $6^4 \cdot 8 \cdot 10$. The topology of **1** is evidently different from those 4-connected topologies of minerals: diamond ($6_2 \cdot 6_2 \cdot 6_2 \cdot 6_2 \cdot 6_2 \cdot 6_2$), NbO ($6_2 \cdot 6_2 \cdot 6_2 \cdot 6_2 \cdot 8_2 \cdot 8_2$), PtS ($4 \cdot 4 \cdot 8_2 \cdot 8_2 \cdot 8_2 \cdot 8_2$), $CdSO_4$ ($6 \cdot 6 \cdot 6_2 \cdot 6 \cdot 6 \cdot \infty$), quartz ($6 \cdot 6 \cdot 6_2 \cdot 6_2 \cdot 8_7 \cdot 8_7$) and $CrB_4$ ($4 \cdot 6_2 \cdot 6 \cdot 6 \cdot 6 \cdot 6$) [27].

The IR spectrum of **1** was collected from a solid sample palletized with KBr in the range of 400–4000 cm$^{-1}$ (Fig. S4) and displays four characteristic vibration bands resulting from the Keggin-type POM framework at 947, 895, 765 and 699 cm$^{-1}$, which are assigned to $\nu(W\text{–}O_t)$, $\nu(Si\text{–}O_a)$, $\nu(W\text{–}O_b)$ and $\nu(W\text{–}O_c)$, respectively [25]. In comparison with $K_8[\alpha\text{-}SiW_{11}O_{39}]\cdot 13H_2O$ (Fig. S5), the $\nu_{as}(W\text{–}O_t)$ vibration band for **1** has a red-shift of 8 cm$^{-1}$, indicating that interactions between $[Cu(dap)_2(H_2O)]^{2+}$, $[Cu(dap)_2]^{2+}$ cations and the terminal oxygen atoms of $[\alpha\text{-}SiW_{11}CuO_{39}]^{6-}$ fragments are weak, which is well consistent with the long Cu–O distances of 2.523(23)–3.106(22) Å. The $\nu(W\text{–}O_c)$ vibration bands for **1** split into three peaks, the possible major reason for which may be related to the fact that the incorporation of the Cu$^{II}$ cations to the defect sites of the $[\alpha\text{-}SiW_{11}O_{39}]^{8-}$ fragments leads to the deformation and distortion of the $[\alpha\text{-}SiW_{11}O_{39}]^{8-}$ skeletons. Apparently, the IR spectrum of **1** greatly differs from that of $Na_{10}[A\text{-}\alpha\text{-}SiW_9O_{34}]\cdot 18H_2O$ (Fig. S6), which further suggests the evolution from $[A\text{-}\alpha\text{-}SiW_9O_{34}]^{10-}$ to $[\alpha\text{-}SiW_{11}O_{39}]^{8-}$ in the formation of **1**. The $\nu(NH_2)$ and $\nu(CH_2)$ stretching vibration resonances are observed at 3138 and 2925 cm$^{-1}$ whereas the $\delta(NH_2)$ and $\delta(CH_2)$ bending vibration signals appear at 1588 cm$^{-1}$ and 1459 cm$^{-1}$, which verifies the presence of dap ligands. The vibration band centered at 3433 cm$^{-1}$ is indicative of lattice water molecules or coordination water molecules in **1**.

The TG analysis of **1** was measured on crystalline samples under $N_2$ atmosphere from 25 to 750 °C (Fig. S7). The TG curve indicates that **1** loses weight in two steps between 25 and 750 °C. The weight loss of 2.00% in the first step from 25 to 100 °C corresponds to the liberation of two lattice water molecules and two coordination water molecules (calcd. 2.09%). Above 100 °C, the second weight loss of 12.41% up to 750 °C is observed and assigned to the removal of six dap ligands (calcd. 12.91%).

POM electrochemistric properties have recently attracted considerable interest due to their potentials in electrocatalytic processes and the manufacture of chemically modified electrodes [28]. It is shown that POMs can deliver electrons to other species and serve as the powerful electron reservoirs for multi-electron reductions and electrocatalytic processes [29]. Thus, the solid-state electrochemical and

electrocatalytic properties of **1** have been measured by cyclic voltammetry (CV) in 0.5 mol·L$^{-1}$ $Na_2SO_4 + H_2SO_4$ aqueous solution by entrapping it in a carbon paste electrode (CPE). The CV curve of **1** in a pH = 0.46 sulfate medium at a scan rate of 50 mV·s$^{-1}$ at room temperature is illustrated in Fig. 2a. It can be clearly perceived that the CV pattern in the potential range of −0.8 to 0.4 V exhibits four pairs of redox waves and their half-wave potentials $E_{1/2} = (E_{pa} + E_{pc})/2$ are −0.018 V, −0.342 V, −0.446 V and −0.636 V (vs the Ag/AgCl electrode), respectively. The (I–I′) redox wave designates the redox process of the $Cu^{II}$ centers [30] and the peak potential separation of 245 mV indicates that the redox process of the $Cu^{II}$ centers is irreversible. Another three pairs of redox waves (II–II′), (III–III′) and (IV–IV′) are attributed to the redox process of the $W^{VI}$ centers in the polyoxoanion framework [31] and their peak potential separations are 37 mV, 75 mV and 149 mV, which respectively correspond to the reversible two-electron, reversible one-electron and semi-reversible one-electron charge-transfer processes. Fig. 2b shows the variation of cathodic (II) peak current intensities of the $W^{VI}$-based wave with the scan rates. When the scan rates vary from 20 to 110 mV s$^{-1}$, the peak current intensities ($I$) are proportional to the scan rates ($\upsilon$) and its linear equation is $I = 0.00002\upsilon + 0.00007$ with the correlation coefficient of 0.9858, which indicates that the redox process at **1**-CPE is diffusion-controlled [32].

In recent years, POM-based materials have been extensively investigated in electrocatalytic reduction because of the ability to undergo reversible multi-electron redox processes [33]. For instance, Keita et al. studied that two-electron-reduced $[SiMo_{12}O_{40}]^{4-}$can reduce nitrite in acidic solution [34]; Peng et al. evaluated the electrocatalytic activity of $(pbpy)_4H[PMo_{12}O_{40}(VO)]$-CPE and $(pbpy)_4H_4[SiMo_{12}O_{40}]$-CPE for the reduction of chlorate [33]. Thus, the activities of **1**-CPE toward the electrocatalytic reduction of nitrite and bromate have been probed in 0.5 mol·L$^{-1}$ $Na_2SO_4 + H_2SO_4$ aqueous solution (pH = 0.46). It is well known that nitrite is a common pollutant from agricultural or industrial processes and the direct electroreduction needs a high overpotential at the electrode surface and no obvious response is observed at a bare CPE [35]. We find that **1**-CPE displays the electrocatalytic activity toward the reduction of $NO_2^-$ in the acidic sulfate medium in the range of −0.8 to 0.4 V. As shown in Fig. 2c, it can be clearly observed that, with addition of nitrite, the reduction peak current intensities of the $Cu^{II}$-based wave are less affected whereas the reduction peak current intensities of the $W^{VI}$-based wave increase gradually and the corresponding oxidation peak current intensities decrease gradually. This phenomenon manifests that the reduction of nitrite is primarily mediated by the reduced species of tungsten-oxo clusters in **1**. Actually, such phenomenon has been also previously encountered [28]. In addition, bromate acts as a suspicious human carcinogen [36] and is used as a food additive [37], therefore, it is very meaningful to monitor or remove it. In general, the reduction of bromate is totally irreversible at a glassy carbon electrode in acidic aqueous solution and does not occur prior to the evolution of hydrogen [29]. Previous experiments have verified that the reduction of bromate can readily be catalyzed by the mixed-valence tungsten species [38]. To test the electrocatalytic ability of **1**-CPE toward the reduction of $BrO_3^-$, the CV behavior of **1**-CPE in 0.5 mol·L$^{-1}$ $Na_2SO_4 + H_2SO_4$ aqueous solution containing various concentrations of $NaBrO_3$ has been performed at room temperature (Fig. 2d). With addition of $BrO_3^-$, the anodic peak currents of the $W^{VI}$-based wave decrease while the corresponding cathodic peak currents gradually rise, however, the peak currents of the $Cu^{II}$-based wave are almost unaffected. This phenomenon indicates that the catalytic reduction process of $BrO_3^-$ is triggered by the $W^{VI}$-based wave. From the above statements we can know that **1**-CPE shows obvious electrocatalytic activities for the nitrite and bromate reduction.

In summary, a unique 3-D mono-$copper^{II}$ substituted ST **1** has been hydrothermally synthesized and structurally characterized. **1** represents the first 3-D ST framework with the O'Keeffe vertex symbol of $6 \cdot 8_2 \cdot 6 \cdot 6 \cdot 10_2 \cdot 6$ in POM chemistry. Its solid-state electrochemical and electro-catalytic properties have been performed and discussed. The results indicate that the **1**-CPE has obvious electrocatalytic activities toward the nitrite and bromate reduction. In the following time, the further work in this area will be dedicated to prepare chiral POM-based materials with ferroelectricity and piezoelectricity by introducing chiral organic ligands to the reaction system.

## Acknowledgments

This work was supported by the Natural Science Foundation of China (21101055, 21301049, U1304208), the Natural Science Foundation of Henan Province (122300410106, 102300410093), the Foundation of State Key Laboratory of Structural Chemistry (20120013), the 2014 Special Foundation for Scientific Research Project of Henan University, the 2012 Young Backbone Teachers Foundation from Henan Province and the Students Innovative Pilot Plan of Henan University (2013, 2014).

## Appendix A. Supplementary material

CCDC 1016093 for **1** contains the supplementary crystallographic data for this paper. These data can be obtained free of charge from the Cambridge Crystallographic Data Centre via www.ccdc.cam.ac.uk/data_request/cif. Supplementary data associated with this article can be found, in the online version, at doi: http://dx.doi.org/10.1016/j.inoche.2014.10.003. These data include MOL files and InChiKeys of the most important compounds described in this article.

## References

[1] A. Dolbecq, E. Dumas, C.R. Mayer, P. Mialane, Hybrid organic–inorganic polyoxometalate compounds: from structural diversity to applications, Chem. Rev. 110 (2010) 6009.
[2] Z.M. Zhang, S. Yao, Y.G. Li, Y.H. Wang, Y.F. Qi, E.B. Wang, New trimeric polyoxotungstate aggregates based on $[P_2W_{12}O_{48}]^{14-}$ building blocks, Chem. Commun. (2008) 1650.
[3] S.G. Mitchell, C. Streb, H.N. Miras, T. Boyd, D.L. Long, Leroy Cronin, Face-directed self-assembly of an electronically active Archimedean polyoxometalate architecture, Nat. Chem. 2 (2010) 308.
[4] L.J. Chen, D.Y. Shi, J.W. Zhao, Y.L. Wang, P.T. Ma, J.P. Wang, J.Y. Niu, Three transition-metal substituted polyoxotungstates containing Keggin fragments: from trimer to one-dimensional chain to two-dimensional sheet, Cryst. Growth Des. 11 (2011) 1913.
[5] B.S. Bassil, M. Ibrahim, R. Al-Oweini, M. Asano, Z. Wang, J. van Tol, N.S. Dalal, K.Y. Choi, R.N. Biboum, B. Keita, L. Nadjo, U. Kortz, A planar $\{Mn_{19}(OH)_{12}\}^{26+}$ unit incorporated in a 60-tungsto-6-silicate polyanion, Angew. Chem. Int. Ed. 50 (2011) 5961.
[6] H.S. Liu, J. Peng, Z.M. Su, Y.H. Chen, B.X. Dong, A.X. Tian, Z.G. Han, E.B. Wang, Synthesis and structural characterization of sandwich-type Keggin-γ-lacunary silicotungstates with an open Wells–Dawson-like structure, Eur. J. Inorg. Chem. (2006) 4827.
[7] B.S. Bassil, S.S. Mal, M.H. Dickman, U. Kortz, H. Oelrich, L. Walder, 6-Peroxo-6-zirconium crown and its hafnium analogue embedded in a triangular polyanion: $[M_6(O_2)_6(OH)_6(\gamma\text{-}SiW_{10}O_{36})_3]^{18-}$ (M = Zr, Hf), J. Am. Chem. Soc. 130 (2008) 6696.
[8] S.G. Mitchell, P.I. Molina, S. Khanra, H.N. Miras, A. Prescimone, G.J.T. Cooper, R.S. Winter, E.K. Brechin, D.L. Long, R.J. Cogdell, L. Cronin, A mixed-valence manganese cubane trapped by inequivalent trilacunary polyoxometalate ligands, Angew. Chem. Int. Ed. 50 (2011) 9154.
[9] L. Yang, Y. Huo, J.Y. Niu, Combination between $[B\text{-}\alpha\text{-}SiW_9O_{34}]$ unit and triangular inorganic $Ni_6$ core under hydrothermal conditions: from monomer to rare dimer with malposed dodeca-nickel centers, Dalton Trans. 42 (2013) 364.
[10] L.B. Ni, F. Hussain, B. Spingler, S. Weyeneth, G.R. Patzke, Lanthanoid-containing open Wells–Dawson silicotungstates: synthesis, crystal structures, and properties, Inorg. Chem. 50 (2011) 4944.
[11] K. Suzuki, M. Sugawa, Y. Kikukawa, K. Kamata, K. Yamaguchi, N. Mizuno, Strategic design and refinement of Lewis acid base catalysis by rare-earth-metal-containing polyoxometalates, Inorg. Chem. 51 (2012) 6953.
[12] S.Z. Li, D.D. Zhang, Y.Y. Guo, P.T. Ma, X.Y. Qiu, J.P. Wang, J.Y. Niu, Keggin polyoxoanion supported organic–inorganic trinuclear lutetium cluster, $\{Na(H_2O)_3[Lu(pydc)(H_2O)_3]_3\}[SiW_{12}O_{40}]\cdot 26.5H_2O$, Dalton Trans. 41 (2012) 9885.
[13] G. Hervé, A. Tézé, Study of α- and β-enneatungstosilicates and germinates, Inorg. Chem. 16 (1977) 2115.
[14] J.W. Zhao, J. Luo, L.J. Chen, J. Yuan, H.Y. Li, P.T. Ma, J.P. Wang, J.Y. Niu, Novel 1-D double-chain organic–inorganic hybrid polyoxotungstates constructed from dimeric copper–lanthanide heterometallic silicotungstate units, CrystEngComm 14 (2012) 7981.
[15] J. Luo, J.W. Zhao, J. Yuan, Y.Z. Li, L.J. Chen, P.T. Ma, J.P. Wang, J.Y. Niu, An organic–inorganic hybrid 1-D double-chain copper–yttrium heterometallic silicotungstate $[Cu(dap)_2(H_2O)]_2\{Cu(dap)_2[\alpha\text{-}H_2SiW_{11}O_{39}Y(H_2O)_2]_2\}\cdot 10H_2O$, Inorg. Chem. Commun. 27 (2013) 2713.

[16] J. Luo, C.L. Leng, L.J. Chen, J. Yuan, H.Y. Li, J.W. Zhao, Three 3D organic–inorganic hybrid heterometallic polyoxotungstates assembled from 1:2-type $[Ln(\alpha\text{-}SiW_{11}O_{39})_2]^{13-}$ silicotungstates and $[Cu(dap)_2]^{2+}$ linkers, Synth. Met. 162 (2012) 1558.

[17] S.B. Tian, Y.Z. Li, J.W. Zhao, P.T. Ma, L.J. Chen, A novel organic–inorganic hybrid sandwich-type germanotungstate with discrete $[Fe_4(en)_2(\alpha\text{-}GeW_9O_{34})_2]^{8-}$ polyoxoanions and 1-D $[Fe_4(en)\ (\alpha\text{-}GeW_9O_{34})_2]_n^{8n-}$ polymeric chains, Inorg. Chem. Commun. 33 (2013) 99.

[18] J.W. Zhao, D.Y. Shi, L.J. Chen, X.M. Cai, Z.Q. Wang, P.T. Ma, J.P. Wang, J.Y. Niu, Two organic–inorganic hybrid 1-D and 3-D polyoxotungstates constructed from hexa-$Cu^{II}$ substituted sandwich-type arsenotungstate units, CrystEngComm 14 (2012) 2797.

[19] Crystal data for **1**: $C_{18}H_{68}Cu_4N_{12}O_{43}SiW_{11}$, $Mr = 3445.44$, tetragonal, space $I4_1cd$, $a = 34.3990(16)$, $b = 34.3990(16)$, $c = 21.3501(19)$ Å, $V = 25263(3)$ Å$^3$, $Z = 16$, $D_c = 3.623$ g·cm$^{-3}$, $\mu = 21.376$ mm$^{-1}$, $F(000) = 24768$, $GOOF = 1.019$. Of 63029 total reflections collected, 11019 were unique [$R_{int} = 0.1130$, $R_1(wR_2) = 0.0633(0.1382)$] for 582 parameters and 7678 reflections [$I > 2\sigma(I)$]. Diffraction data were collected on a Bruker Smart APEX II CCD diffractometer with graphite-monochromated Mo Kα radiation (λ = 0.71073 Å) at 296(2) K. The structure was solved by direct methods and refined by full-matrix least squares on $F^2$ using the SHELXTL–97 program package. Intensity data were corrected for Lorentz and polarization effects as well as for multi-scan absorption. No hydrogen atoms associated with water molecules were located from the difference Fourier map. All of the non-hydrogen atoms except for some C, N and O atoms were refined anisotropically. Positions of the hydrogen atoms attached to the carbon and nitrogen atoms were geometrically placed. All hydrogen atoms were refined isotropically as a riding mode using the default SHELXTL parameters.

[20] I.D. Brown, D. Altermatt, Bond-valence parameters obtained from a systematic analysis of the inorganic crystal structure database, Acta Crystallogr. B41 (1985) 244.

[21] H.H. Thorp, Bond valence sum analysis of metal-ligand bond lengths in metalloenzymes and model complexes, Inorg. Chem. 31 (1992) 1585.

[22] K. Yu, Y.G. Li, B.B. Zhou, Z.H. Su, Z.F. Zhao, Y.N. Zhang, A basket-like $[Sr \subset P_6Mo^{V}{}_4Mo^{VI}{}_{14}O_{73}]^{10-}$ polyoxoanion modified with $\{Cu(phen)(H_2O)_x\}$ (x = 1–3) fragments: synthesis, structure, magnetic and electrochemical properties, Eur. J. Inorg. Chem. 2007 (2007) 5662.

[23] J.W. Zhao, Y.Z. Li, F. Ji, J. Yuan, L.J. Chen, G.Y. Yang, Syntheses, structures and electrochemical properties of a class of 1-D double chain polyoxotungstate hybrids $[H_2dap][Cu(dap)_2]_{0.5}[Cu\ (dap)_2(H_2O)][Ln(H_2O)_3(\alpha\text{-}GeW_{11}O_{39})]\cdot 3H_2O$, Dalton Trans. 43 (2014) 5694.

[24] J.W. Zhao, S.T. Zheng, G.Y. Yang, 0-D and 1-D inorganic–organic composite polyoxotungstates constructed from in-situ generated monocopper$^{II}$-substituted Keggin polyoxoanions and copper$^{II}$–organoamine complexes, J. Solid State Chem. 181 (2008) 2205.

[25] J.P. Wang, J.W. Zhao, X.Y. Duan, J.Y. Niu, Syntheses and structures of one- and two-dimensional organic–inorganic hybrid rare earth derivatives based on monovacant Keggin-type polyoxotungstates, Cryst. Growth Des. 6 (2006) 507.

[26] O.V. Dolomanov, A.J. Blake, N.R. Champness, M. Schröder, OLEX: new software for visualization and analysis of extended crystal structures, J. Appl. Crystallogr. 6 (2003) 1283.

[27] M. O'Keeffe, M. Eddaoudi, H. Li, T. Reineke, O.M. Yaghi, Section 1: tutorial frameworks for extended solids: geometrical design principles, J. Solid State Chem. 152 (2000) 3.

[28] B. Keita, P. de Oliveira, L. Nadjo, U. Kortz, The ball-shaped hetero-polytungstates $[\{Sn(CH_3)_2(H_2O)\}_{24}\{Sn(CH_3)_2\}_{12}(A\text{-}XW_9O_{34})_{12}]^{36-}$ (X = P, As): stability, redox and electrocatalytic properties in aqueous media, Chem. Eur. J. 13 (2007) 5480.

[29] X. Wang, E. Wang, Y. Lan, C. Hu, Renewable $PMo_{12}$-based inorganic–organic hybrid material bulk-modified carbon paste electrode: preparation, electrochemistry and electrocatalysis, Electroanal 14 (2002) 1116.

[30] J.E. Toth, F.C. Anson, Electrocatalytic reduction of nitrite and nitric oxide to ammonia with iron-substituted polyoxotungstates, J. Am. Chem. Soc. 111 (1989) 2444.

[31] B. Keita, L.J. Nadjo, New aspects of the electrochemistry of heteropolyacids: part IV. Acidity dependent cyclic voltammetric behaviour of phosphotungstic and silicotungstic heteropolyanions in water and N,N-dimethylformamide, J. Electroanal. 227 (1987) 77.

[32] M. Sadakane, E. Streckhan, Electrochemical properties of polyoxometalates as electrocatalysts, Chem. Rev. 98 (1998) 219.

[33] Z. Han, Y. Zhao, J. Peng, Y. Feng, J. Yin, Q. Liu, The electrochemical behavior of Keggin polyoxometalate modified by tricyclic, aromatic entity, Electroanal 17 (2005) 1097.

[34] B. Keita, A. Belhouari, L. Nadjo, R. Contant, Electrocatalysis by polyoxometalate/polymer systems: reduction of nitrite and nitric oxide, J. Electroanal. Chem. 381 (1995) 243.

[35] X. Wang, H. Hu, A. Tian, H. Lin, J. Li, Application of tetrazole-functionalized thioethers with different spacer lengths in the self-assembly of polyoxometalate-based hybrid compounds, Inorg. Chem. 49 (2010) 10299.

[36] M.M. Moore, T. Chen, Mutagenicity of bromate: implications for cancer risk assessment, Toxicology 221 (2006) 190.

[37] L.M. Rodriguez-Albelo, A.R. Ruiz-Salvador, A. Sampieri, D.W. Lewis, A. Gómez, B. Nohra, P. Mialane, J. Marrot, F. Sécheresse, C. Mellot-Draznieks, R.N. Biboum, B. Keita, L. Nadjo, A. Dolbecq, Zeolitic polyoxometalate-based metal–organic frameworks (Z-POMOFs): computational evaluation of hypothetical polymorphs and the successful targeted synthesis of the redox-active Z-POMOF1, J. Am. Chem. Soc. 131 (2009) 16078.

[38] B. Wang, S.J. Dong, Electrocatalytic properties of mixed-valence molybdenum oxide thin film modified microelectrodes, Electroanal. Chem. 379 (1994) 207.